ARTICLE IN PRESS

Ceramics International xxx (xxxx) xxx

Contents lists available at ScienceDirect

Ceramics International

journal homepage: www.elsevier.com/locate/ceramint

Practical guidance for easily interpreting the emission and physicochemical parameters of Eu^{3+} in solid-state hosts

Pablo Serna-Gallén *, Héctor Beltrán-Mir, Eloísa Cordoncillo

Departamento de Química Inorgánica y Orgánica, Universitat Jaume I, Av. Vicent Sos Baynat s/n, 12071, Castelló de la Plana, Spain

ARTICLE INFO

Handling Editor: P. Vincenzini

Keywords:
Europium
Lanthanides
Emission spectra
Luminescence
Solid state

ABSTRACT

Materials doped with the luminescent Eu^{3+} ion are attracting an ever-increasing amount of attention due to their potential applications in solid-state lighting, display devices, solar cells, or bioanalytics. But, why Eu^{3+}? Unlike other lanthanides, its electronic features make the calculation of some physicochemical parameters quite straightforward, since they can be extracted directly from the emission spectrum. Highly appreciated for its reddish emission, the luminescent ion has also been widely used as a site-sensitive structural probe. With this in mind, this paper aims to offer easy guidance with helpful advice on how to interpret measurements of the emission spectra. It also presents the most useful tools for saving time, and gives a focused and practical explanation of the theoretical concepts involved.

1. Introduction

The term luminescence (from Latin *lumen* and *essentia*) was coined in 1888 by the physicist Eilhard Wiedemann to distinguish incandescence (emission of light caused by heat) from other physical phenomena in which the emission of light did not depend exclusively on a rise in temperature [1]. When it comes to photoluminescence (a result of the de-excitation of absorbed photons), the trivalent europium ion (Eu^{3+}) emerges as a crucial lanthanide (Ln^{3+}) due to its top-notch optical properties.

The application of Eu^{3+}-doped materials, especially inorganic solids, covers a vast range of areas such as solid-state lighting, display devices, solar cells, optical detectors, medical imaging, and tumor detection, inter alia [2–4]. The current energy scenario comprises a globally increasing demand, with prices skyrocketing, and problems to guarantee a reliable supply of energy that is starting to have a significant impact on socio-economic welfare [5]. This situation has pushed the scientific community to become more committed than ever to developing cutting-edge materials, and energy-saving and energy-efficient technologies, with a particular focus on solid-state illumination [6,7].

The vast majority of papers, reviews, or books about Ln^{3+} luminescence are intended for specialist audiences and experienced spectroscopists, and leave non-experts struggling to follow them. To overcome this, in the past decade, two reviews have been published about the interpretation and comprehension of some misconceptions concerning the emission spectra of Eu^{3+}-doped materials [8,9]. The detailed studies offer a good explanation of some interesting physical parameters of Eu^{3+} and structural properties, and provide examples of different compounds (complexes, hybrids, oxides, etc.). However, they do not go deeply enough into the common problems that scientists can find in a laboratory routine.

Given the foregoing, this review intends to offer practical, easy guidance for researchers, with helpful advice in all the sections, as well as presenting the most promising tools (free software packages, databases, examples, etc.) that can save them a lot of time in the calculation of some physicochemical parameters (phonon energies and refractive indices of the host lattices, color coordinates, branching ratios, asymmetry ratio, and Judd Ofelt parameters). In addition, to facilitate a better comprehension of the physics involved, every section has a short theoretical background that starts from a basic knowledge perspective and raises possible questions that scientists may come up with. Therefore, let scientists record the emission spectrum and *Fiat lux*.

2. Electronic features

2.1. Energy levels

The electronic configuration of Eu^{3+} is $[Xe]4f^6$. The 4*f* electrons can be arranged in different microstates in the seven 4*f* orbitals. These microstates are grouped into different terms of energy whose degeneracy is

* Corresponding author.
E-mail address: pserna@uji.es (P. Serna-Gallén).

https://doi.org/10.1016/j.ceramint.2023.01.141
Received 4 December 2022; Received in revised form 11 January 2023; Accepted 15 January 2023
Available online 19 January 2023
0272-8842/© 2023 The Authors. Published by Elsevier Ltd. This is an open access article under the CC BY-NC-ND license (http://creativecommons.org/licenses/by-nc-nd/4.0/).

Please cite this article as: Pablo Serna-Gallén, *Ceramics International*, https://doi.org/10.1016/j.ceramint.2023.01.141

given by the expression $(2S + 1)(2L + 1)$, where S is the total spin quantum number and L is the total orbital angular momentum quantum number.

In addition, the degeneracy of terms can be lost because of spin-orbit coupling, and a new parameter is introduced: J, the total angular quantum momentum, which takes values from $|L + S|$, $|L + S| - 1$, (…), to $|L - S|$. So, each value of J gives a different level of energy. If crystal-field effects are considered, these energy levels can also be divided into sublevels, commonly called Stark levels [10]. Fig. 1(a) depicts an energy diagram showing the different Eu^{3+} free-ion levels without considering the crystal-field effects because they depend on the host material. As an example, Fig. 1(b) highlights the theoretical Stark splitting of the $^7F_0$ levels of Eu^{3+}-doped KPb_2Cl_5 with C_2/C_s site symmetry as reported by C. Cascales et al. [11]. The energy values were obtained from Refs. [11,12].

2.2. Some basics about symmetry and electronic transitions

In spectroscopy, electronic transitions are governed by selection rules, which determine whether such transitions can occur or not. By far one of the most widely known is the Laporte selection rule, which essentially states that for a transition to be allowed in centrosymmetric systems, the parity of the electronic states involved must change [13]. Understanding this selection rule from a theoretical point of view commonly requires a profound solid basis in quantum mechanics and group theory, as usually found in the literature [14]. With this in mind, this paper intends to offer a proper view of the fundamentals of electronic transitions without entering into details in great depth.

The probability of an electronic transition occurring is related to the transition moment integral:

$$\int_{-\infty}^{\infty} \Psi_i^* \vec{\mu} \Psi_f \, d\tau = \langle \Psi_i | \vec{\mu} | \Psi_f \rangle \tag{1}$$

where Ψ_i and Ψ_f are the wave functions of the initial and final states, respectively, $\vec{\mu}$ is the transition moment operator, and $d\tau$ is the volume element. If this integral is zero, such electronic transition will not occur (it is forbidden). If the integral has a non-zero value, however, the transition will be allowed [15].

In order to know whether a transition is allowed or not, it is just necessary to determine the symmetry of the transition moment function $\Psi_i^* \vec{\mu} \Psi_f$. Considering the symmetry labels for the initial (Γ_i) and final (Γ_f) states, and for the operator of the transition being considered (Γ_μ), the direct product can be expressed as:

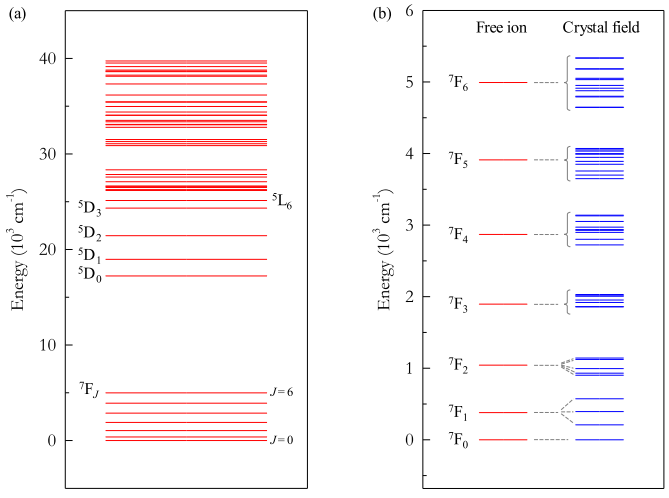

Fig. 1. (a) Energy level diagram for the Eu^{3+} free-ion (not considering crystal field effects). (b) Example of the Stark splitting of the $^7F_0$ levels due to the crystal field effect in a Eu^{3+}-doped sample of KPb_2Cl_5.

$$\Gamma_i \otimes \Gamma_\mu \otimes \Gamma_f \tag{2}$$

For the transition to be allowed, the decomposition of the direct product must strictly contain the totally symmetric irreducible representation Γ_1 (which is even with respect to all symmetry operations). Γ_1 can be denoted on a character table by one of the following Mulliken symbols: A, A′, A_g, A_1, A_1' or A_{1g}, depending on the symmetry group. Note that when considering centrosymmetric systems (with gerade, g, even symmetry) $\Gamma_1 \equiv A_g$ or A_{1g} [16,17].

The 4*f* orbitals of lanthanide ions have u (ungerade, odd) symmetry, see Fig. 2. Therefore, for intraconfigurational transitions (4*f*-4*f* transitions), we obtain that $\Gamma_i \otimes \Gamma_f \equiv u \otimes u = g$. Consequently, the viability of the transition taking place depends on the symmetry (parity) of the transition moment operator $\vec{\mu}$, which is linked to the character of each electronic transition. If $\vec{\mu}$ has u symmetry, then the direct product yields an ungerade symmetry ($\Gamma_1 \equiv u \otimes g = u$) and the transition is forbidden, since the corresponding decomposition cannot contain the gerade A_g/ A_{1g} term. In contrast, if $\vec{\mu}$ has g symmetry, the direct product yields a gerade symmetry ($\Gamma_1 \equiv g \otimes g = g$) and the transition is allowed, a priori. However, when considering the site symmetry of the Eu^{3+} ion embedded in the host lattice, it might be possible to obtain a gerade symmetry but with a term different to A_g/ A_{1g} such as E_g or B_{1g}, thus making the transition forbidden.

Additionally, it is worth mentioning the relevance of polarized measurements in the acquisition of the emission spectrum of Eu^{3+}-doped anisotropic crystals with non-cubic lattices. In these experiments, the emitted light is polarized and the presence of the emission bands is subjected to the site symmetry that occupies the dopant in the lattice and the corresponding selection rules [9]. In this case, the transition moment function would be defined by $\Psi_i^* \vec{\mu}_\alpha \Psi_f$, with $\alpha = x,y,z$, depending on the polarization. If the operators $\vec{\mu}_x$, $\vec{\mu}_y$, and $\vec{\mu}_z$ have different irreducible representations, the selection rules for different linearly polarized light are distinguishable. Further details can be found in Ref. [18].

2.3. Understanding the character of electronic transitions in lanthanides

Depending on their dipole nature, we can group the electronic transitions of Ln^{3+} ions into three types: electric dipole (ED), magnetic dipole (MD), and electric quadrupole (EQ) transitions [9].

Most of the transitions observed in the luminescence spectra of Ln^{3+} ions are *electric dipole transitions*. Such a transition arises as a consequence of the interaction of the lanthanide ion with the electric field component of light by generating an electric dipole. The creation of a dipole involves a linear motion of the charge. The electric dipole operator $\vec{P}$ has u symmetry. Therefore, intraconfigurational ED transitions

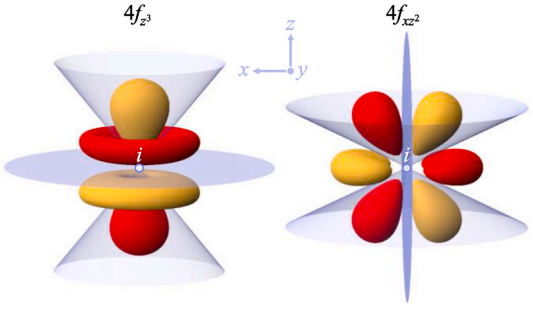

Fig. 2. Shape of two 4*f* atomic orbitals highlighting in lilac the planar and conical nodes, whose interjection point generates the inversion center (*i*). Yellow zones represent regions where the wave function Ψ is positive, while the red regions denote negative values. *f* orbitals are ungerade, since the symmetry operation $\hat{i}\Psi(x,y,z) \neq -\Psi(x,y,z)$, where $\hat{i}$ is the symmetry operator of *i*. (For interpretation of the references to color in this figure legend, the reader is referred to the Web version of this article.)

are forbidden. Notwithstanding, when the Ln^{3+} ions are subjected to a crystal field, the selection rules are relaxed and the transitions become partially allowed. One of the main contributions of this relaxation is ascribed to the *J*-mixing effect, which points out that states with different *J* quantum numbers can be mixed due to the crystal field potential and can lead to a change in the energy level positions [19]. From a theoretical point of view, these mixed states are reflected on the expression of the crystal-field Hamiltonian because additional terms are introduced. As the ED transitions observed in the luminescence spectra of lanthanides come about as a result of a perturbation, they are weaker than ordinary (or free-ion) ED transitions, so they are usually called *induced electric dipole transitions*.

On the other hand, *magnetic dipole transitions* originate from the interaction of the lanthanide ion with the magnetic field component of light by generating a magnetic dipole. Magnetic dipole radiation can be visualized as a rotational displacement of the charge. Since the direction of rotation does not change when applying an inversion with respect to an inversion center, the magnetic dipole operator $\vec{M}$ has *g* symmetry and, therefore, 4*f*-4*f* magnetic dipole transitions are allowed. Moreover, the intensity of this type of transition is relatively independent of the environment of the Ln^{3+} ion in the crystal lattice. This independency is ascribed to the fact that no crystal field effects are expected to affect MD transitions since the magnetic susceptibility (in a nonmagnetic medium) is the same as for vacuum. Consequently, the crystal field wave functions are not needed in the calculation of the intensities of MD transitions and only the free-ion wave functions are considered. Thus, a simple cubic dependence of the MD transition rate, A_{MD}, can be established with the refractive index of the material, *n* [20–22].

Finally, *electric quadrupole transitions* arise from charge displacement with a quadrupole nature. An electric quadrupole consists of four-point charges with a net charge and dipole moment equal to zero. We can visualize it as two dipoles joined in such a way that their dipole moments cancel each other out [23]. The electric quadrupole operator $\vec{Q}$ has *g* symmetry and EQ transitions are allowed. However, although there are theoretical calculations that postulate the existence of these transitions, there is still no experimental evidence supporting them. For better comprehension, Fig. 3 plots the electric dipole $\vec{P}$, magnetic dipole $\vec{M}$, and electric quadrupole $\vec{Q}$ moments for a particular distribution of point charges.

3. Some useful considerations about the emission spectra

3.1. General assignment of the bands

In an emission spectrum of Eu^{3+}, the bands observed are commonly associated with the $^5D_0 \rightarrow {}^7F_J$ transitions, since $^5D_0$ is the metastable and lowest-lying excited state. Emissions from higher excited states ($^5D_{1,2,3}$) to the ^7F_J levels can also be detected in some crystal matrices, although low phonon energy is required, as will be addressed later on. Thus, for the vast majority of researchers, special interest must be paid to $^5D_0 \rightarrow {}^7F_J$ transitions, especially for $J = 0$–4, since the $^5D_0 \rightarrow {}^7F_{5,6}$ ED transitions ($\lambda_{em} > 750$ nm) are hardly ever detected with conventional spectrofluorometers due to sensitivity reasons [24]. Table 1 summarizes the character of the main transitions and the approximate region of the emission spectrum in which the corresponding bands usually appear (in wavelength, wavenumber, and eV units) [25–27]. It has also to be mentioned that due to the crystal field effect generated by the surrounding ions of Eu^{3+} in the host lattice, the $^5D_0 \rightarrow {}^7F_J$ transitions can have different components depending on the site symmetry, as will be discussed later in Section 6. An example of this splitting has been illustrated previously in Fig. 1(b).

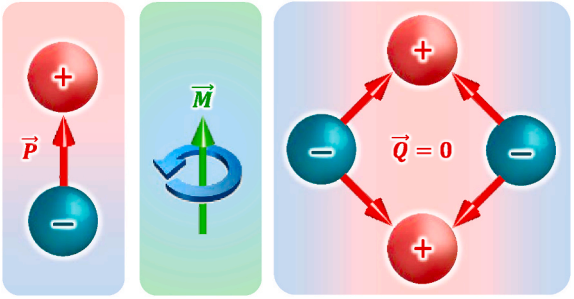

Fig. 3. Schematic representation of the electric ($\vec{P}$) and magnetic ($\vec{M}$) dipole moment, and electric quadrupole ($\vec{Q}$) moment for a distribution of point charges.

3.2. The phonon energy and how to properly discriminate emissions from higher excited states

Most of the compounds containing Eu^{3+} possess a reddish emission due to the presence of $^5D_0 \rightarrow {}^7F_J$ transitions. In a common excitation spectrum of Eu^{3+} (which is recorded fixing the emission wavelength), the band corresponding to the $^7F_0 \rightarrow {}^5L_6$ transition (≈395 nm) usually has the highest intensity (without considering possible charge transfers from the host lattice). According to the energy level diagram depicted previously in Fig. 1, when Eu^{3+} ions are excited to the $^5L_6$ state, rapid non-radiative multiphonon relaxations usually occur and Eu^{3+} ions reach the metastable and lowest-lying excited state ($^5D_0$), from which the transitions to the ^7F_J ground state manifold take place [28]. Therefore, as this de-excitation process is fast, the luminescence from the upper ^5D_J states is not usually observed [29]. The presence of bands associated with emissions from the higher excited states ($^5D_{1,2,3}$) critically depends upon two factors: (1) the phonon energy of the host lattice, and (2) the concentration of Eu^{3+} ions.

The cut-off phonon energy of a host lattice can be ascribed to the highest-energy vibrational mode. Ideal host materials should therefore have low lattice phonon energies to avoid luminescent quenching processes and reach high quantum yields. Host materials containing heavy halides (Cl, Br, I) display very low cut-off phonon energies (generally below 300 cm^{-1}), but their hygroscopic nature and low chemical stability prevent them from being applied to practical uses. On the other hand, oxides exhibit good chemical stability, although they commonly present higher phonon energies (>550 cm^{-1}) and consequently the quantum yields tend to be low [30]. In contrast, fluoride-based materials not only have good chemical stability but also low phonon energies (300–550 cm^{-1}), which makes them exceptional host materials for luminescent ions [31,32]. Table 2 summarizes the cut-off phonon energy of some common host lattices used for Ln^{3+} doping [33–35]. For the specific examples, most of the values were obtained from the JARVIS-DFT database [36]. This repository is focused on density functional theory (DFT) predictions of material properties, especially for crystalline materials. JARVIS-DFT is a part of the NIST-JARVIS project (National Institute of Standards and Technology-Joint Automated Repository for Various Integrated Simulations). This database and tools since they contain very useful information for the description of host lattices, especially taking into account their (electro/thermo)dynamic features.

On this basis, host lattices with low phonon energy that also contain low doping concentrations of trivalent europium will probably exhibit

Table 1
Band assignment of the main electronic transitions of Eu^{3+} and dipole character.

Transition	Character	λ_{em} (nm)	Energy (cm^{-1})	Energy (eV)
$^5D_0 \rightarrow {}^7F_0$	ED	580	17,250	2.15
$^5D_0 \rightarrow {}^7F_1$	MD	590	16,700	2.10
$^5D_0 \rightarrow {}^7F_2$	ED	615	16,300	2.00
$^5D_0 \rightarrow {}^7F_3$	ED	650	15,400	1.90
$^5D_0 \rightarrow {}^7F_4$	ED	690	14,500	1.80

Table 2
Cut-off phonon energy (PE) of some common host lattices used for Ln^{3+} doping and some specific examples.

Host lattice	PE (cm^{-1})	Example	PE (cm^{-1})
Borate	1300–1400	YBO_3	1300
Phosphate	1000–1200	YPO_4	1050
Silicate	900–1100	$Y_2Si_2O_7$	1060
Vanadate	800–900	YVO_4	890
Titanate	600–800	$CaTiO_3$	640
Aluminate	600–800	$YAlO_3$	650
Simple oxide	550–900	Y_2O_3	600
Indium-based oxide	450–600	$CaIn_2O_4$	475
Oxyfluoride	400–600	YOF	470
Fluoride	300–550	YF_3	475
Chloride	200–300	YCl_3	260
Bromide	170–250	YBr_3	215
Iodide	150–200	YI_3	190

emission lines from the different ^5D_J excited states covering the whole visible spectral region that can yield a global white light emission: $^5D_3$ (blue), $^5D_2$ (blue-green), $^5D_1$ (green-yellow), and $^5D_0$ (orange-red) [37]. As an example, Fig. 4 shows the emission spectrum of 1 mol% Eu^{3+}-doped $CaIn_2O_4$ prepared by X. Liu et al. [38].

Furthermore, as previously outlined, another substantial aspect to take into account is the Eu^{3+} concentration in the material. If the concentration is high, the Eu^{3+}–Eu^{3+} distance shortens and cross-relaxation phenomena become more probable. This non-radiative process involves partial energy transfer between two neighboring Eu^{3+} ions in the crystal lattice. Thus, the energy emission is quenched in favor of the lower energy level emission according to different mechanisms [39,40]. In order to make this physical process easier to understand, Fig. 5 depicts different schemes regarding the cross-relaxation process that can occur from the different excited states between two Eu^{3+} ions. The energy levels of each ion are represented in different colors (red and blue) and the partial energy diagrams have been plotted so as to visualize the similarity between the energy gaps at first glance.

After addressing the main concepts concerning the emission from higher excited states, one of the major problems to face is how to discriminate these emissions and properly assign the corresponding bands of the whole emission spectrum of a Eu^{3+}-doped sample. When emissions from all the ^5D_J excited states (or some of them) take place, the mixing (convolution) of some bands is expected due to the small energy difference of different transitions, especially in the yellow-orange region of the spectrum, where the significant $^5D_0 \rightarrow {}^7F_{1,2}$ transitions appear. The simplest way to discriminate the transitions occurring from the higher excited states ($^5D_{1,2,3}$) from those occurring from the lowest-lying excited state ($^5D_0$) is to record the emission spectrum of a sample at different detector delay times (DT). Increasing the DT will suppress the emissions from the $^5D_{1,2,3}$ higher energy states, since they have shorter lifetimes in comparison with transitions from the $^5D_0$ ground state.

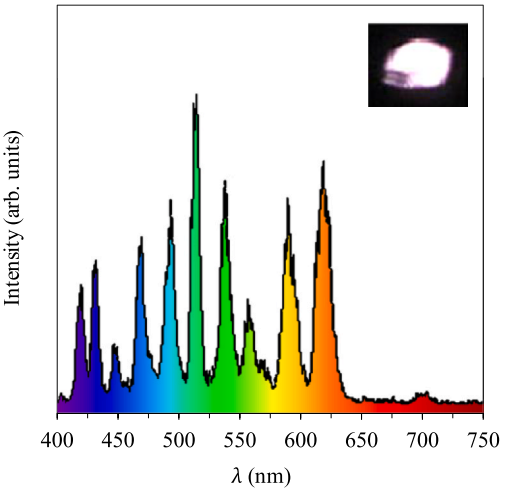

Fig. 4. Emission spectrum of 1 mol% Eu^{3+}-doped $CaIn_2O_4$ recorded under an excitation wavelength of 397 nm. The inset shows a luminescent photograph with the resulting white light emission. Adapted with permission from Ref. [38].

As an example, Fig. 6 shows the emission spectra of α-KY_3F_{10} powder doped with 1 mol% Eu^{3+} [41]. With a DT = 0.2 ms, the spectrum exhibits a complex behavior due to the mixing of $^5D_{0-3} \rightarrow {}^7F_J$ transitions. However, when the DT is increased to 10 ms, only the contribution of $^5D_0 \rightarrow {}^7F_J$ transitions is observed. See, for instance, the difference in the peak splitting in the yellow-orange region of the spectrum (three components with DT = 0.2 ms, and two components with DT = 10 ms).

3.3. The emission color: CIE xy coordinates

In Solid State Science, the description and quantification of the emission color of a phosphor are of paramount relevance, since it allows comparison with other materials and provides a direct connection with the luminescence spectral features. The color of any visible light emission can be illustrated using the CIE (*Commission Internationale de l'Eclairage*) 1931 chromaticity diagram, also known as the CIE *xy* diagram, which is a universally accepted system for representing the composition of color through three primary colors (blue, green, and red) [42,43].

The calculation of color coordinates is based on the formulations of the CIE system set up in 1931. As color is three-dimensional, it can be characterized by an (x, y, z) set, where the different coordinates correspond to the red, green, and blue components, respectively. Notwithstanding, given that $x + y + z = 1$, it is enough to define an (x, y) pair to represent the color in a plane (2D) graph, since the z coordinate can be inferred from the other two. The white light emission point is located at the center of a CIE *xy* diagram, Fig. 7, with chromatic coordinates x = 0.33 and y = 0.33 [44,45].

The *xy* coordinates can be calculated from the emission spectrum of a phosphor using different equations described in the literature [46]. However, sometimes it can be time-consuming but different free software packages and computational tools are available online. Some useful examples are: GoCIE [47], CIE Coordinate Calculator (works with a MATLAB routine) [48], and Chromaticity Diagram (a complement to be used in Origin) [49]. The file containing the emission spectrum data can be uploaded, the chromatic coordinates are calculated, and they can also be plotted in a CIE diagram.

4. The asymmetry ratio

4.1. Determination of the branching ratios

A theoretical approach for branching ratios can be used to predict the intensity of different emission lines [50]. However, most of the emphasis is commonly placed on the experimental branching ratios (β_J), which can be obtained directly from the emission spectra of the lanthanide ion taking into account the relative areas of the bands. For example, considering the $^5D_0 \rightarrow {}^7F_J$ transitions of Eu^{3+}, the general expression for β_J is:

$$\beta_J = \frac{I_{0J}}{\sum I_{0J}} \tag{3}$$

where I_{0J} is the integrated intensity of the $^5D_0 \rightarrow {}^7F_J$ transition.

Once the different β_J have been calculated, several physicochemical parameters can be obtained. As regards studies about Eu^{3+} luminescence in the literature, the most calculated and discussed parameter is the asymmetry ratio (R). Europium is highly appreciated among the scientific community due to its feature of acting as a symmetry-sensitive

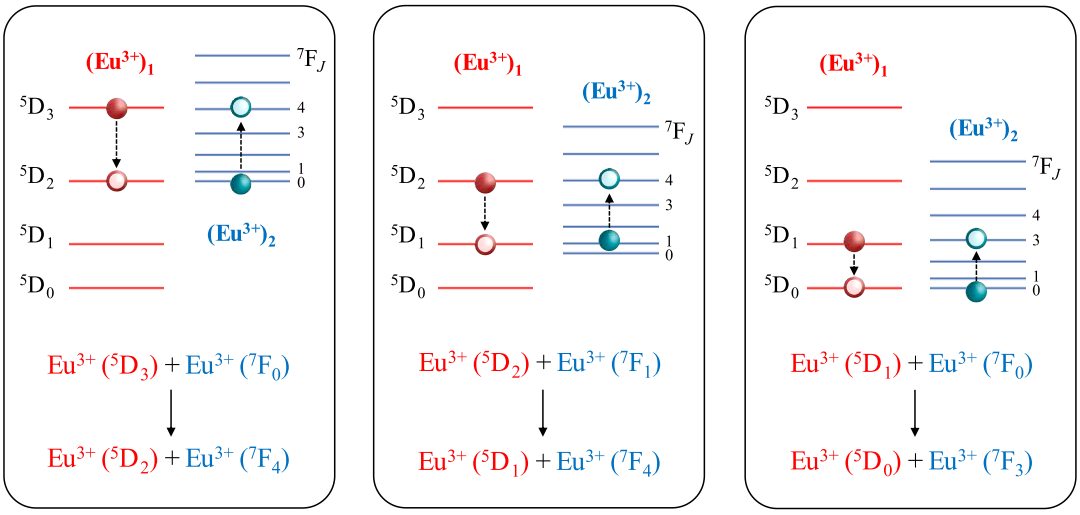

Fig. 5. Possible cross-relaxation mechanisms occurring between two neighboring Eu^{3+} ions in the crystal lattice.

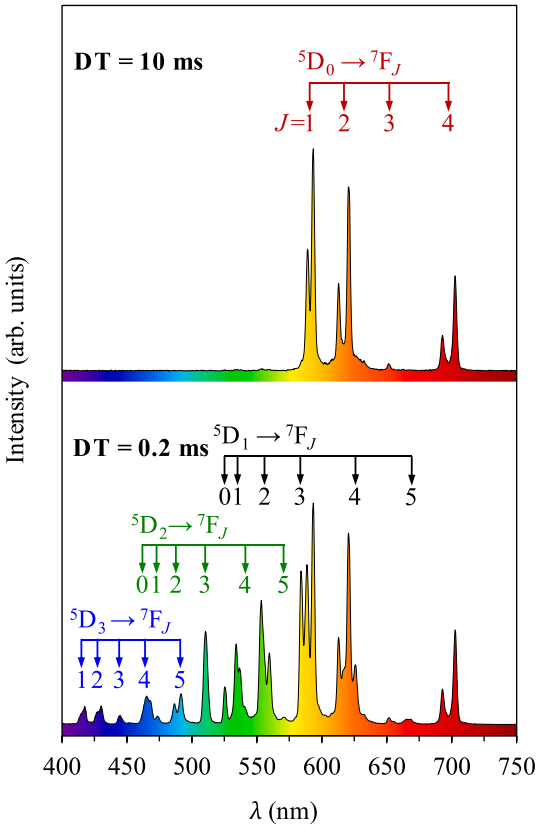

Fig. 6. Emission spectra obtained with delay times (DT) of 0.2 and 10 ms upon excitation at 395 nm for 1 mol% Eu^{3+}-doped α-KY_3F_{10}. Reprinted with permission from Ref. [41].

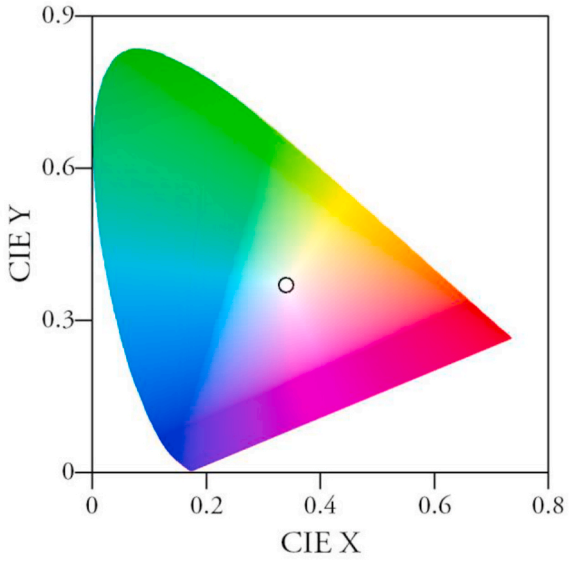

Fig. 7. CIE chromaticity diagram. The white light emission point is located at its center (indicated with an empty circle in the figure).

spectroscopic probe, as will be discussed later on. The intensity of the $^5D_0 \rightarrow {}^7F_1$ MD transition is relatively independent of the site symmetry of Eu^{3+} ions, while the $^5D_0 \rightarrow {}^7F_2$ ED transition has a hypersensitive character, i.e., it is affected to a large extent by the surroundings and crystal field of Eu^{3+} [51]. Therefore, the asymmetry ratio can shed some light on the local environment of this particular lanthanide. Defining I_{02} and I_{01} as the integrated intensity of the $^5D_0 \rightarrow {}^7F_2$ and $^5D_0 \rightarrow {}^7F_1$ transitions, respectively, R can be extracted from the branching ratios:

$$R = \frac{I_{02}}{I_{01}} = \frac{\beta_2}{\beta_1} \tag{4}$$

It is important to note that researchers must avoid the calculus of this parameter using absolute intensities of the bands rather than integrated intensities.

4.2. The Jacobian transformation: to do, or not to do

The most common way of recording and presenting the signal data of absorption, emission, or excitation spectra as a function of the electromagnetic spectrum is in wavelength units. However, from a physical point of view, the data should be presented as a function of energy for the cases in which the quantitative analysis of the emission spectra is required. Converting wavelength to energy units (e.g., eV) is quite straightforward using the familiar equation:

$$E = \frac{h\,c}{\lambda} \tag{5}$$

where h is Planck's constant and c, the speed of light in vacuum.

Expressing h in eV·s, c in nm·s^{-1}, and λ in nm, the above expression results in:

$$E\ (\mathrm{eV}) = \frac{1239.84}{\lambda\ (\mathrm{nm})} \tag{6}$$

Although it might appear that with this transformation everything is solved, it must be recalled that a change in the units of the abscissa axis must also imply a conversion of the signal values (intensity), if not, the integrated area under the curve will differ [52]. This conversion of $I(\lambda)$ to $I(E)$ is called Jacobian transformation. Then, in order to express the signal values properly, the following operation must be applied:

$$I(E) = I(\lambda)\frac{h\,c}{E^2} = I(\lambda)\frac{\lambda^2}{h\,c} = I(\lambda)\frac{\lambda(\mathrm{nm})^2}{1239.84} \tag{7}$$

At this point, the question that probably comes to mind is whether or not the Jacobian transformation should be performed to calculate the asymmetry ratio accurately, since it is derived from integrated areas.

The use of the Jacobian transformation in an emission spectrum with narrow bandwidth peaks, as is normally the case for Ln^{3+}-doped materials, does not have any prominent effects. However, if the spectra have broad bands, this transformation plays a crucial role and must be applied. For further details, see the work of Mooney and Kambhampati addressing this issue [53]. To prove that the Jacobian transformation is not usually required in well-defined emission spectra of Eu^{3+}, Fig. 8 presents the same data in different units and the resulting asymmetry ratio value. As highlighted, the difference in the value of R (0.02) is more than negligible. To summarize, the Jacobian transformation can be neglected for the calculation of the asymmetry ratio in the majority of cases.

4.3. Avoid emissions from higher excited states

As previously discussed in Section 3.2, when a Eu^{3+}-doped sample exhibits emission lines corresponding to transitions from higher excited states ($^5D_{1,2,3}$), the emission spectra should also be recorded increasing the DT of the detector so as to effectively suppress the contribution of these transitions. If this experiment is not carried out, substantial errors can be made in the calculation of some physicochemical parameters of Eu^{3+}. To underscore this fact, Fig. 9 (Fig. 6 magnified in the region of interest) depicts the emission spectra of a sample recorded at two different DT. The values of the asymmetry ratio change notably (0.21).

4.4. "Unexpected" values and controversy about the asymmetry ratio

A broad statement in the literature about the asymmetry ratio is that the higher the R values are, the more deviation of the Eu^{3+} site from a centrosymmetric geometry there is. In other words, low values of the asymmetry ratio are expected, a priori, when Eu^{3+} ions are located in

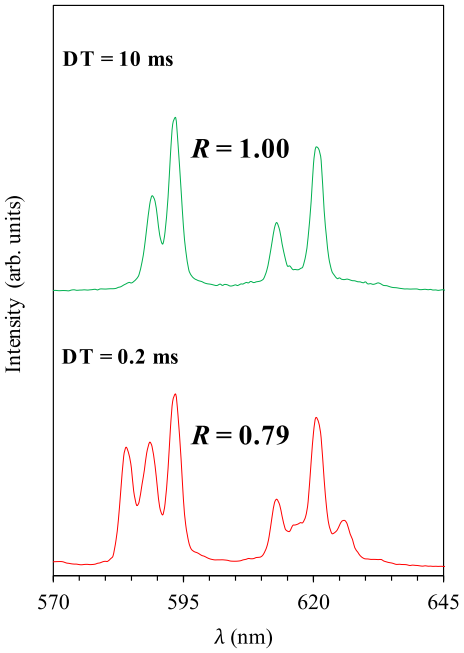

Fig. 9. Emission spectra obtained with a delay time (DT) of 0.2 and 10 ms upon excitation at 395 nm for 1 mol% Eu^{3+}-doped α-KY_3F_{10}.

crystal sites with an inversion center [54]. The detailed works of Tanner [8] and Binnemans [9] highlighted that distortions or deviations from the centrosymmetric geometry of Eu^{3+} generally increase R, but great caution must be paid when comparing the asymmetry ratios of different crystal structures because the $^5D_0 \rightarrow {}^7F_2$ transition probability also depends on the shape of the coordination polyhedra (as well as the coordination number), and the nature of the ligands (or surrounding ions) [55]. Therefore, sometimes it can be obtained "unexpected" R values (very small or large) that do not follow the incorrect general statement of the asymmetry ratio tendency.

A good example can be found considering Eu^{3+}-doped YF_3. In the orthorhombic YF_3 crystal structure, Y^{3+} ions are located at a site with C_s symmetry (which is also the crystallographic symmetry for Eu^{3+} ions replacing Y^{3+}). Of course, C_s is a low symmetry point group (only σ_h and E operations are possible), and without an inversion center. Hence, one could wrongly expect to obtain high R values (higher than unity, since the lack of an inversion center could imply the domination of the $^5D_0 \rightarrow {}^7F_2$ transition in the emission spectrum), but asymmetry ratio values in the range 0.3–0.5 are obtained [41,56,57]. In fluoride-based materials, it has been quite common to find that the $^5D_0 \rightarrow {}^7F_1$ MD transition dominates over the $^5D_0 \rightarrow {}^7F_2$ ED transition. The explanation

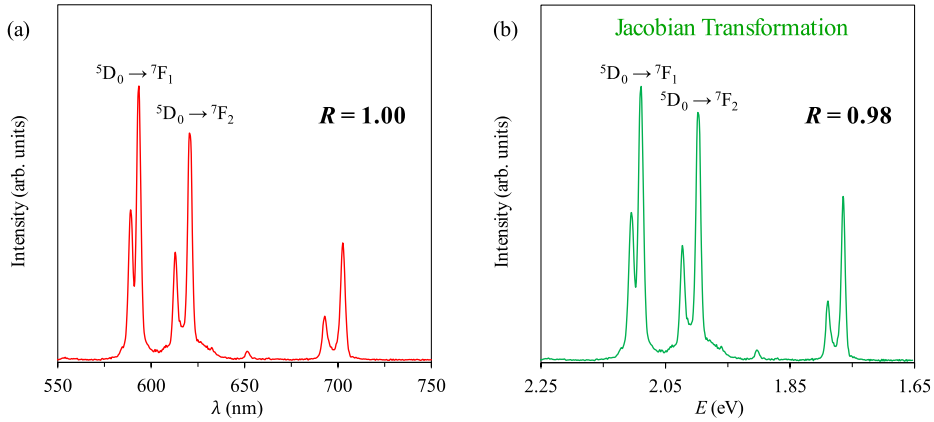

Fig. 8. Emission spectra of 1 mol% Eu^{3+}-doped α-KY_3F_{10} presented in (a) wavelength and (b) energy units. The asymmetry ratio is indicated for both cases.

lies in the high ionicity of Eu–F bonds, which allows only a little admixture of opposite parity states to the Eu^{3+} *f*-states, and it makes the ED transition less favorable and thus with low intensity [58].

Hence, it would be wrong stating that Eu^{3+} ions are located at centrosymmetric sites in orthorhombic YF_3 due to the low *R* values obtained.

5. Judd Ofelt parameters of Eu^{3+}

5.1. Theory and applications: a 60-year history

Occasionally, history is witness to unprecedented, peculiar, unique coincidences in science, as was the appearance of the Judd Ofelt (JO) theory 60 years ago. On August 1, 1962, two independent papers (by two authors who had never met in person) saw the light simultaneously: Brian R. Judd published his work *Optical Absorption Intensities of Rare-Earth Ions* in the journal Physical Review [59], while George S. Ofelt's paper entitled *Intensities of Crystal Spectra of Rare-Earth Ions* appeared in The Journal of Chemical Physics [60]. These two articles have been considered a breakthrough in the field of rare-earth spectroscopy. They laid the foundations of what we now know as the JO theory, which in essence is the most powerful tool in optical spectroscopy for the theoretical calculation and prediction of physicochemical parameters of lanthanides and actinides in solids and solutions. The great advantage of the JO theory is that physical parameters such as dipole oscillator strengths, emission intensities, radiative lifetimes, or quantum efficiencies can be calculated by simply using three material-dependent parameters (the famous JO parameters Ω_2, Ω_4, and Ω_6) and material-independent squared reduced matrix elements of the unit tensor operator connecting the levels of the transitions of interest (abbreviated as U^2, U^4, and U^6) [61,62]. The values of U^λ ($\lambda = 2, 4, 6$) have been tabulated [63,64] and are widely considered invariant for a given Ln^{3+} ion because the position of the *J* levels is weakly affected by the surrounding ions/atoms [65].

After this brief introduction, one could ask oneself: what is the practical application of the JO parameters in Eu^{3+}-doped materials? Does this theory deserve its prestige? The answer is an unequivocal "yes". Since the appearance of those two initial pieces of research, a plethora and constantly growing number of papers have been published. To support this phenomenon, Fig. 10(a) shows the number of papers including the word "Judd Ofelt" published over the years as determined by Scopus (accessed in October 2022). Perhaps the most outstanding feature is the rapid growth of use of this theory for Eu^{3+}-doped compounds, as highlighted in Fig. 10(b). The number of papers published was also determined by Scopus by combining the word "Judd Ofelt" with "europium", "Eu", or "Eu^{3+}".

5.2. The particular case of Eu^{3+}

Traditionally, JO parameters are determined from the absorption spectra of Ln^{3+}-doped materials [50]. For the vast majority of rare-earth ions, the calculation of the JO parameters requires a complex mathematical algorithm and also extensive knowledge of quantum mechanics. Readers interested in an in-depth explanation can consult some worthy detailed works in the literature [66,67]. However, the scope of this paper is to provide practical, easy guidance for researchers so they do not have to deal with tedious calculations, rather than just describing the JO equations in full once again, which is something that has already been carried out in many studies.

Unlike other trivalent lanthanide ions, the electronic characteristics of Eu^{3+} make the calculation of the JO parameters quite straightforward, since they can be extracted directly from the emission spectrum. Among all the $^5D_0 \rightarrow {}^7F_J$ transitions, only $^5D_0 \rightarrow {}^7F_1$ has a magnetic dipole character, while the rest of the transitions are (induced) electric dipole, see Table 1. As previously stated, the dipole strength of MD transitions is independent of the environment of the Ln^{3+} ion in the host lattice and can be calculated by theory. The dipole strength is directly related to the emission rate (A_{if}) of a $\Psi_i \rightarrow \Psi_f$ transition. Thus, the emission rate for the $^5D_0 \rightarrow {}^7F_1$ transition is defined as:

$$A_{01} = n^3 \, (A_{01})_{vac} \tag{8}$$

where *n* denotes the refractive index of the material and $(A_{01})_{vac}$ is the MD transition rate in vacuum (14.65 s^{-1}). Such electronic particularity allows us to use this transition as a reference for the rest of the $^5D_0 \rightarrow {}^7F_J$ transitions.

In addition, another important aspect that makes the calculation of Ω_λ quite easy is the fact that all the squared reduced matrix elements U^λ are zero except for the $^5D_0 \rightarrow {}^7F_{2,4,6}$ transitions [68], as outlined in Table 3.

The Ω_2 parameter has been associated with the polarizable and covalent character of the Ln^{3+} ion. Thus, it provides useful information about the crystal environment of Eu^{3+} and is considered a short-range parameter [60,69,70]. The reason why the asymmetry ratio *R* and the Ω_2 parameter in practice provide the same information is that a direct

Table 3
Reduced matrix elements for the $^5D_0 \rightarrow {}^7F_J$ ED transitions of Eu^{3+}.

Transition	U^2	U^4	U^6
$^5D_0 \rightarrow {}^7F_0$	0	0	0
$^5D_0 \rightarrow {}^7F_2$	0.0032	0	0
$^5D_0 \rightarrow {}^7F_3$	0	0	0
$^5D_0 \rightarrow {}^7F_4$	0	0.0023	0
$^5D_0 \rightarrow {}^7F_5$	0	0	0
$^5D_0 \rightarrow {}^7F_6$	0	0	0.0002

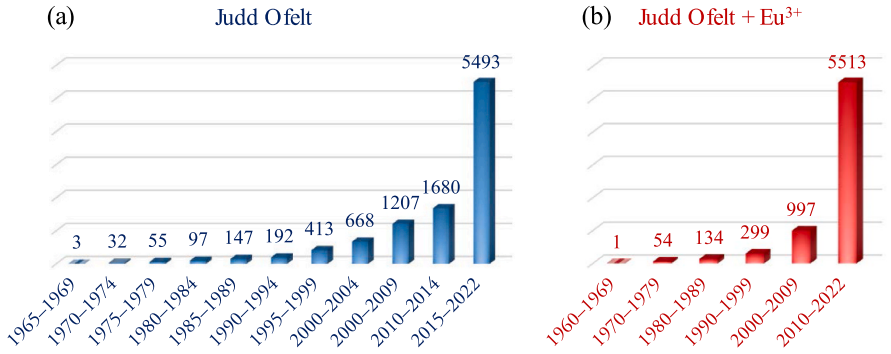

Fig. 10. Number of papers published including the word (a) "Judd Ofelt", and (b) "Judd Ofelt" plus "europium", "Eu", or "Eu^{3+}". Data were extracted from the Scopus database (accessed in October 2022).

relation between them can be derived for a given material:

$$\Omega_2 = kR \quad (9)$$

where k is a constant (see Ref. [71] for further details). Therefore, interpreting the Ω_2 requires the same caution as with the asymmetry ratio in order to avoid misleading conclusions.

Conversely, Ω_4 and Ω_6 show the long-range effects and are affected by the viscosity and rigidity of the host lattice [72], although it is quite complicated to obtain the Ω_6 parameter from the emission spectra due to the instrumental limitations and the low intensity of the $^5D_0 \rightarrow {}^7F_6$ transition. In most cases, this is why only the discussion of Ω_2 and Ω_4 is contemplated for Eu^{3+}-doped materials. It should also be noted that for a correct calculation of the JO parameters from the emission spectrum, the emission from higher excited states, if present, must be suppressed by increasing the DT of the detector, as previously discussed.

5.3. Calculus by computational programs

In this section, the most promising tools are briefly presented to calculate the aforementioned parameters of Eu^{3+} using free software packages available online.

To calculate the physicochemical parameters from the experimental emission spectrum, there are two main application software packages of interest: LUMPAC [73] and JOES [74]. LUMPAC was developed in 2014 and allows the calculation of the JO parameters (Ω_2 and Ω_4), radiative (A_{rad}) and non-radiative (A_{nrad}) emission rates, and quantum efficiencies (η). It must be highlighted that if we are only interested in these parameters, the application interface is very easy. LUMPAC also integrates three additional modules that are devoted to other luminescent features, such as calculating ground state geometries of systems containing Ln^{3+} ions. However, to be able to use these extra modules, it is necessary to work with MOPAC [75] and ORCA [76], which are programs based on semiempirical quantum chemistry that require a higher degree of knowledge about computation.

Some years later, in 2019, the JOES software package was released to complement and improve the existing JO parameterization of the emission spectrum. In addition to the physicochemical parameters obtained by LUMPAC, JOES derives other quantities: the branching ratios (both experimental and theoretical), emission cross-sections (σ_e), and the CIE xy coordinates. It must be highlighted that although the CIE coordinates and diagram can be plotted, we suggest using the previously mentioned GoCIE program for graphical representations because colors, legends, text size/font, and so on can be configured as desired.

As explained above, the Ω_6 parameter is seldom obtained from the emission spectra because the $^5D_0 \rightarrow {}^7F_6$ transition (810–840 nm) is commonly outside the limits of detection of the equipment. Moreover, this transition is also very weak due to the low value of the reduced matrix element U^6 (0.0002) and is therefore practically irrelevant for describing the emission features. Notwithstanding, we must recall that in the absorption and excitation spectra, the $^7F_0 \rightarrow {}^5L_6$ transition (see Section 3.2) tends to be the dominant one. Hence, for these spectra, Ω_6 (which is only related to this transition) has far more relevance. To overcome this problem, recently, in 2022, the JOEX software has been developed [77], which allows calculation of the three JO parameters from the excitation spectrum. Fig. 11 compares the JO parameterization with the corresponding transitions using the excitation and emission spectra.

5.4. No data available for the refractive index

Even though refractive indices for the most common materials can be found in the literature, it could be that some of them are not included in such databases, especially when working with novel materials, different crystal phases, solid solutions, or different doping concentrations. Since the refractive index is required for the calculation of the JO parameter and derivation of other substantial physicochemical parameters, finding an alternative solution is a matter of concern, since having no data available for the refractive index means that no calculations are possible. Herein it is referred a simple theoretical approach that can overcome this problem, without the need to perform ellipsometry measurements that might be complicated for some kinds of materials.

Previous to going deeper into this approach, it is worth mentioning the concept of birefringence, which is defined as the optical property of a material that differs by polarization and light propagation [78]. Birefringence occurs in anisotropic crystals with non-cubic lattices. Therefore, different refractive indices of the materials can be determined depending on the light polarization [79]. Mainly, two types of crystals can be distinguished: uniaxial and biaxial. Uniaxial crystals are characterized by one optical axis and two refractive indices: n_o (ordinary) and n_e (extraordinary). On the other hand, biaxial crystals can be described by two optical axis and three refractive indices: n_x, n_y, and n_z. The calculation of the birefringence for biaxial crystals is complex, while for the uniaxial materials, it is expressed as:

$$\Delta n = n_e - n_o \quad (10)$$

For some crystals, the birefringence value is relevant since it can be in the order 0.1–0.2, as in phosphate-type lattices [80]. After these considerations, the mean refractive index of a material (n) can be calculated for anisotropic crystals as $n = (2n_o + n_e)/3$ for uniaxial crystals, and $n = (n_x + n_y + n_z)/3$ for biaxial crystals [81].

The mean refractive index of a compound can be calculated following the procedure described by Shannon and Fischer using the Anderson-Eggleton equation, which is based on ion polarizabilities [81–83]. They calculated the polarizability parameters from data recorded at a wavelength of 589.3 nm. Therefore, the equations yield the mean refractive indices at 589.3 nm. However, the spectral region in which the $^5D_0 \rightarrow {}^7F_{1,2,4}$ transitions occur (600–700 nm) is very close to 589.3 and only small changes in n values are expected. For most

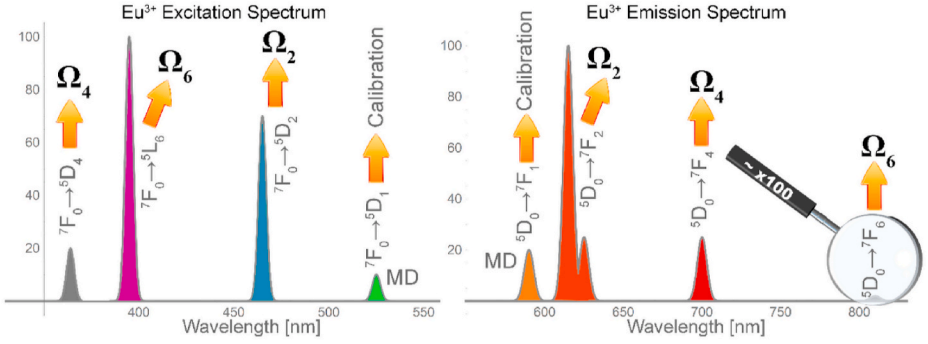

Fig. 11. Comparison of the JO parameterization with the corresponding transitions using the excitation and emission spectra. Reprinted with permission from Ref. [77].

compounds, only the second decimal would be affected and this theoretical approach can be of high relevance. See as an example Fig. 12, which highlights the minor deviation of the refractive index in the 600–700 nm range for a simple oxide (Y_2O_3), complex oxides ($Y_3Al_5O_{12}$, $MgAl_2O_4$), and a fluoride (LaF_3). The values were taken from the Mikhail Polyanskiy database [84].

In order to prove the validity of this method, the theoretical mean refractive indices of the above-mentioned compounds were calculated using the Anderson-Eggleton equation. The crystal structure data were taken from the Springer Materials database [85–88]. The results are summarized in Table 4 and, as highlighted with the relative errors, the theoretical values are extremely close to the reported ones.

6. Inferring the site-selective symmetries of Eu^{3+}

When Eu^{3+} ions are embedded in a host lattice, they usually substitute other cations. This replacement can be isoelectronic (e.g., $Y^{3+} \leftrightarrow Eu^{3+}$ in Y_2O_3) or non-isoelectronic (e.g., $Ca^{2+} \leftrightarrow Eu^{3+}$ in CaF_2, or $Ti^{4+} \leftrightarrow Eu^{3+}$ in TiO_2, which imply the generation of ionic vacancies [89–91]). Quite often, these substitutions produce low deviations in the crystal lattice, breaking the ideal site-symmetry of the host ions. One of the reasons explaining these deviations is the difference in the ionic radius between the host and the dopant ion. To have a better comprehension of the site-substitution, knowing the values of Eu^{3+} ionic radii for different coordination numbers (CN) is of great interest. However, the well-known Shannon's radii database lacks all the values for Eu^{3+} in a CN > 9 [92], which is a drawback since host ions with such CN are quite common in solid-state materials, e.g., $CN(Ca^{2+}) = 12$ in $CaTiO_3$ perovskite. To fill this gap, Jia [93] proposed an empirical formula to calculate the unknown crystal radii of trivalent and divalent rare earth ions with $6 \leq CN \leq 12$. Table 5 shows the ionic radii of Eu^{3+} with different coordination numbers. Apart from that, dopants can also be distributed irregularly in the particles of a compound, resulting in different site occupations. One recurrent example can be found in the interfaces or grain boundaries of a particle, since Eu^{3+} ions occupying their vicinities tend to possess low symmetries and present broad signals and non-well-resolved emission spectra [94,95].

Widely discussed in the literature, the particular features of the trivalent europium ion make it possible to use it as a site-sensitive structural probe. Both the $^5D_0$ and $^7F_0$ states are non-degenerate ($J = 0$). Thus, if the frequency of the pumping excitation source is tuned over the inhomogeneous bandwidth of the $^7F_0$–$^5D_0$ transition, the Stark splitting observed in the emission spectrum will only result from the local crystal field of Eu^{3+} ions situated at a given site with a corresponding point group symmetry [96]. However, it must be highlighted that to record an emission spectrum with high resolution, the temperature must be as low as possible to avoid vibronic contributions. Because of this, the most powerful spectroscopic technique to perform these experiments is laser-induced fluorescence line narrowing (FLN), which requires the use of cryogenic working conditions [97].

Therefore, it is reasonable to infer the site-selective symmetries of Eu^{3+} ions by analyzing the emission profile and the number of Starks components for each $^5D_0 \rightarrow {}^7F_J$ transition (see Table 6). Special attention should be paid to the $^5D_0 \rightarrow {}^7F_{0-4}$ splitting, and care should be taken with the $^5D_0 \rightarrow {}^7F_{5,6}$ transitions because the number of J components observed is usually lower than the predicted ones due to overlapping between the emission lines.

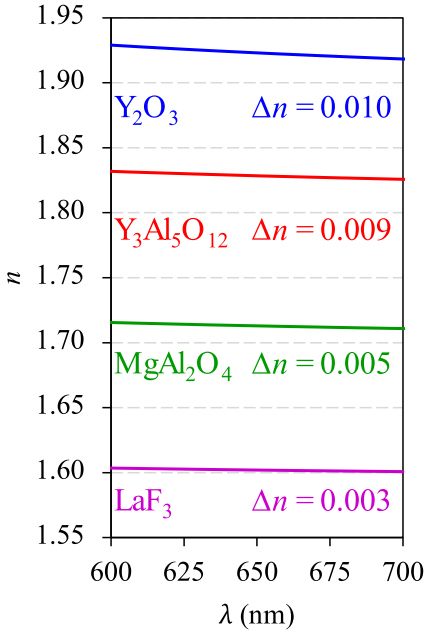

Fig. 12. Evolution and deviation (Δn) of the refractive index in the 600–700 nm range for Y_2O_3, $Y_3Al_5O_{12}$, $MgAl_2O_4$, and LaF_3 compounds.

Table 4
Cell volume of the different host lattices (V_{Cell}), number of formula units (Z), total polarizability (α_T), mean refractive index calculated (n_{calc}) at 589.3 nm, and relative error (δn) in the calculation of n.

Compound	V_{Cell} (Å^3)	Z	α_T (Å^3)	n_{calc}	n_{real}	δn (%)
Y_2O_3	1060.50	16	10.34	1.95	1.93	1.0
$Y_3Al_5O_{12}$	1731.46	8	29.13	1.81	1.83	1.1
$MgAl_2O_4$	542.34	8	8.01	1.71	1.72	0.6
LaF_3	329.98	6	6.04	1.65	1.60	3.1

Table 5
Ionic radii (Å) of Eu^{3+} with different coordination numbers (CN).

CN = 6	CN = 7	CN = 8	CN = 9	CN = 10	CN = 11	CN = 12
0.947	1.01	1.066	1.12	1.17	1.23	1.28

7. Conclusions

In this review, a brief introduction to the electronic features of the luminescent Eu^{3+} ion is first presented in order to lay the foundations for some remarks on optical spectroscopy in Sections 1 and 2. This description is followed by some important symmetry concepts that allow a good comprehension of the character of electronic transitions in lanthanides (ED, MD, and QD).

Section 3 provides some useful insights that help properly interpret the emission spectrum of Eu^{3+}. Aspects discussed include how to assign the bands correctly while being careful to consider possible emissions associated with transitions from higher excited states ($^5D_{1,2,3}$). Detailed information regarding the phonon energy of solid materials with some common examples is also included. Moreover, the cross-relaxation phenomena are discussed in order to have a deeper understanding of the physical processes involved when emissions from different excited states occur. The quantification of the color emission of a phosphor by the CIE xy diagram is presented, focusing on the low time-consuming free software packages available for researchers.

Section 4 gives practical advice about the calculation and interpretation of the asymmetry ratio, which is probably the most discussed parameter in the literature on the Eu^{3+} emission. The asymmetry ratio should be calculated from the emission spectrum with a proper detector delay time, while the Jacobian transformation is not required in most cases. Additionally, a short explanation of some misconceptions about this parameter is also presented.

Section 5 is devoted to the famous Judd Ofelt parameters. After explaining the history and some minor concepts of this theory, it is noted how the explosion of works using this parameter (most of them about Eu^{3+}-doped materials) is mainly due to the electronic peculiarities of

Table 6
Point group assignation according to the number of emission bands of $^5D_0 \rightarrow {}^7F_{0-4}$ transitions. Adapted with permission from Ref. [8].

Symmetry class	Point group	$^7F_0$	$^7F_1$	$^7F_2$	$^7F_3$	$^7F_4$	Symmetry class	Point group	$^7F_0$	$^7F_1$	$^7F_2$	$^7F_3$	$^7F_4$
Icosahedral	I_h	0	1	0	0	0	Tetragonal	C_4	1	2	2	3	5
Cubic	O_h, T_h	0	1	0	0	0		S_4	0	2	3	4	4
	O	0	1	0	1	1		D_{2d}	0	2	2	3	3
	T_d	0	1	1	1	1	Trigonal	D_{3d}, C_{3i}	0	2	0	0	0
	T	0	1	1	2	2		D_3	0	2	2	4	4
Octagonal	D_{4d}	0	2	0	1	2		C_{3v}	1	2	3	3	5
Hexagonal	D_{6h}, C_{6h}	0	2	0	0	0		C_3	1	2	3	5	6
	D_6	0	2	1	2	1	Orthorhombic	D_{2h}	0	3	0	0	0
	C_{6v}, C_6	1	2	2	2	2		D_2	0	3	3	6	6
	D_{3h}	0	2	1	2	3		C_{2v}	1	3	4	5	7
	C_{3h}	0	2	1	3	4	Monoclinic	C_{2h}	0	3	0	0	0
Tetragonal	D_{4h}, C_{4h}	0	2	0	0	0		C_2, C_s	1	3	5	7	9
	D_4	0	2	1	3	3	Triclinic	C_1	1	3	5	7	9
	C_{4v}	1	2	2	2	4		C_i	0	3	0	0	0

this lanthanide. Following on with the practical character of this review, the most interesting computational programs are commented on to facilitate the scientist's work. Attention is also drawn to the methodology presented, which allows the refractive indices of a material to be calculated theoretically when there is no data available.

Finally, Section 6 briefly reviews some interesting facts and advice about the utility of using Eu^{3+} as a site-sensitive structural probe that can be useful for understanding the structure-property relation of a material.

Declaration of competing interest

The authors declare that they have no known competing financial interests or personal relationships that could have appeared to influence the work reported in this paper.

Acknowledgments

This work was supported financially by the Spanish MCIN (Grant PID2020-116149 GB-I00 funded by MCIN/AEI/10.13039/501100011033) and the Universitat Jaume I (Project UJI-B2019-41). P. Serna also thanks the Spanish MCIN for an FPU predoctoral contract (FPU18/04511 funded by MCIN/AEI/10.13039/501100011033 and by "ESF Investing in your future").

References

[1] B. Valeur, M.N. Berberan-Santos, A brief history of fluorescence and phosphorescence before the emergence of quantum theory, J. Chem. Educ. 88 (2011) 731–738, https://doi.org/10.1021/ed100182h.
[2] J. Song, C. Zhang, C. Xu, Y. Qiang, A. Lu, L. Han, Structure and luminescent properties of Eu^{3+}-doped phosphate glass for display device applications, Appl. Phys. Mater. Sci. Process 128 (2022) 1–10, https://doi.org/10.1007/s00339-022-05775-8.
[3] H. Groult, J. Ruiz-Cabello, J. Pellico, A.V. Lechuga-Vieco, R. Bhavesh, M. Zamai, E. Almarza, I. Martín-Padura, E. Cantelar, M.P. Martínez-Alcázar, F. Herranz, Parallel multifunctionalization of nanoparticles: a one-step modular approach for in vivo imaging, Bioconjugate Chem. 26 (2015) 153–160, https://doi.org/10.1021/bc500536y.
[4] B. Song, M. Li, J. Ren, Q. Liu, X. Wen, W. Zhang, J. Yuan, A multifunctional nanoprobe based on europium(III) complex-Fe_3O_4 nanoparticles for bimodal time-gated luminescence/magnetic resonance imaging of cancer cells in vitro and in vivo, New J. Chem. 46 (2022) 9658–9665, https://doi.org/10.1039/d2nj00511e.
[5] A. Omri, F. Belaïd, Does renewable energy modulate the negative effect of environmental issues on the socio-economic welfare? J. Environ. Manag. 278 (2021), 111483 https://doi.org/10.1016/j.jenvman.2020.111483.
[6] R. Devi, R. Boddula, J. Tagare, A.B. Kajjam, K. Singh, S. Vaidyanathan, White emissive europium complex with CRI 95%: butterfly vs. triangle structure, J. Mater. Chem. C 8 (2020) 11715–11726, https://doi.org/10.1039/d0tc02724c.
[7] B. Verma, R.N. Baghel, D.P. Bisen, N. Brahme, V. Jena, Structural, luminescent properties and Judd-Ofelt analysis of $CaMgSiO_4$:Eu^{3+} phosphor for solid state lighting, Opt. Mater. 123 (2022), 111787, https://doi.org/10.1016/j.optmat.2021.111787.
[8] P.A. Tanner, Some misconceptions concerning the electronic spectra of tri-positive europium and cerium, Chem. Soc. Rev. 42 (2013) 5090–5101, https://doi.org/10.1039/c3cs60033e.
[9] K. Binnemans, Interpretation of europium(III) spectra, Coord. Chem. Rev. 295 (2015) 1–45, https://doi.org/10.1016/j.ccr.2015.02.015.
[10] R. Reisfeld, Optical properties of lanthanides in condensed phase, theory and applications, AIMS Materials Science 2 (2015) 37–60, https://doi.org/10.3934/matersci.2015.2.37.
[[11]] C. Cascales, J. Fernández, R. Balda, Investigation of site-selective symmetries of Eu^{3+} ions in KPb_2Cl_5 by using optical spectroscopy, Opt Express 13 (2005) 2141–2152, https://doi.org/10.1364/OPEX.13.002141.
[12] K. Binnemans, A comparative spectroscopic study of Eu^{3+} in crystalline host matrices, Bull. Soc. Chim. Belg. 105 (1996) 793–798.
[13] O. Laporte, W.F. Meggers, Some rules of spectral structure, J. Opt. Soc. Am. Rev. Sci. Instrum. 11 (1925) 459–463. http://www.osapublishing.org/abstract.cfm?uri=josa-12-6-547.
[14] M.S. Dresselhaus, G. Dresselhaus, A. Jorio, Group Theory. Application to the Physics of Condensed Matter, Springer, 2008, https://doi.org/10.1007/978-3-540-32899-8.
[15] R.C. Maurya, J.M. Mir, Molecular Symmetry and Group Theory. Approaches in Spectroscopy and Chemical Reactions, De Gruyter, 2019.
[16] A. De Bettencourt-Dias, Introduction to lanthanide ion luminescence, in: A. De Bettencourt-Dias (Ed.), Luminescence of Lanthanide Ions in Coordination Compounds and Nanomaterials, Wiley, 2014, pp. 1–48, https://doi.org/10.1002/9781118682760.ch01.
[17] I. Gutman, O.E. Polansky, Mathematical Concepts in Organic Chemistry, Springer, 1986, https://doi.org/10.1515/9783112570180.
[18] Y. Wang, G. Yu, M. Rösner, M.I. Katsnelson, H.Q. Lin, S. Yuan, Polarization-dependent selection rules and optical spectrum atlas of twisted bilayer graphene quantum dots, Phys. Rev. X. 12 (2022), 21055, https://doi.org/10.1103/PhysRevX.12.021055.
[19] A.S. Souza, M.A. Couto Dos Santos, The J-mixing effect in Ln^{3+} ions crystal field levels, Chem. Phys. Lett. 521 (2012) 138–141, https://doi.org/10.1016/j.cplett.2011.10.060.
[20] G. Nienhuis, C.T.J. Alkemade, Atomic radiative transition probabilities in a continuous medium, Phys. B+C 81 (1976) 181–188, https://doi.org/10.1016/0378-4363(76)90256-4.
[21] C. Görller-Walrand, L. Fluyt, A. Ceulemans, W.T. Carnall, Magnetic dipole transitions as standards for Judd-Ofelt parametrization in lanthanide spectra, J. Chem. Phys. 95 (1991) 3099–3106, https://doi.org/10.1063/1.460867.
[22] Z. Wang, T. Senden, A. Meijerink, Photonic effects for magnetic dipole transitions, J. Phys. Chem. Lett. 8 (2017) 5689–5694, https://doi.org/10.1021/acs.jpclett.7b02558.
[23] N. Papasimakis, V.A. Fedotov, V. Savinov, T.A. Raybould, N.I. Zheludev, Electromagnetic toroidal excitations in matter and free space, Nat. Mater. 15 (2016) 263–271, https://doi.org/10.1038/nmat4563.
[24] M. Upasani, Synthesis of $Y_3Al_5O_{12}$:Eu and $Y_3Al_5O_{12}$:Eu,Si phosphors by combustion method: comparative investigations on the structural and spectral properties, J. Adv.Cream. 5 (2016) 344–355, https://doi.org/10.1007/s40145-016-0208-y.
[25] Y.-C. Li, Y.-H. Chang, Y.-F. Lin, Y.-S. Chang, Y.-J. Lin, Synthesis and luminescent properties of Ln^{3+} (Eu^{3+}, Sm^{3+}, Dy^{3+})-doped lanthanum aluminum germanate $LaAlGe_2O_7$ phosphors, J. Alloys Compd. 439 (2007) 367–375, https://doi.org/10.1016/j.jallcom.2006.08.269.
[26] C. Görller-Walrand, K. Binnemans, Chapter 167 Spectral intensities of *f-f* transitions, in: J.K.A. Gschneidner, E. LeRoy (Eds.), Handbook on the Physics and Chemistry of Rare Earths, Elsevier, 1998, pp. 101–264, https://doi.org/10.1016/S0168-1273(98)25006-9.
[27] J.-C.G. Bünzli, S.V. Eliseeva, Basics of lanthanide photophysics, in: P. Hänninen, H. Härmä (Eds.), Lanthanide Luminescence, Springer, 2010, pp. 1–45, https://doi.org/10.1007/4243_2010_3.
[28] A. Jose, T. Krishnapriya, T.A. Jose, C. Joseph, N.V. Unnikrishnan, P.R. Biju, Effective sensitization of Eu^{3+} ions on Eu^{3+}/Nd^{3+} co-doped multicomponent borosilicate glasses for visible and NIR luminescence applications, Ceram. Int. 47 (2021) 6790–6799, https://doi.org/10.1016/j.ceramint.2020.11.022.

[29] M. Dejneka, E. Snitzer, R.E. Riman, Blue, green and red fluorescence and energy transfer of Eu^{3+} in fluoride glasses, J. Lumin. 65 (1995) 227–245, https://doi.org/10.1016/0022-2313(95)00073-9.
[30] F. Wang, X. Liu, Rare-earth doped upconversion nanophosphors, in: D.L. Andrews, R.H. Lipson, T. Nann (Eds.), Comprehensive Nanoscience and Nanotechnology, Elsevier Ltd., 2019, pp. 359–384, https://doi.org/10.1016/B978-0-12-812295-2.00146-X.
[31] A. Gulzar, J. Xu, P. Yang, F. He, L. Xu, Upconversion processes: versatile biological applications and biosafety, Nanoscale 9 (2017) 12248–12282, https://doi.org/10.1039/c7nr01836c.
[32] P. Serna-Gallén, H. Beltrán-Mir, E. Cordoncillo, Tuning the optical and photoluminescence properties of high efficient Eu^{3+}-doped KY_3F_{10} phosphors by different synthetic approaches, Opt Laser. Technol. 136 (2021), https://doi.org/10.1016/j.optlastec.2020.106734.
[33] G. Gao, A. Turshatov, I.A. Howard, D. Busko, R. Joseph, D. Hudry, B.S. Richards, Up-conversion fluorescent labels for plastic recycling: a review, Advanced Sustainable Systems 1 (2017), 1600033, https://doi.org/10.1002/adsu.201600033.
[34] X. Tian, C. Wang, J. Wen, S. Lian, C. Ji, Z. Huang, Z. Chen, H. Peng, S. Wang, J. Li, J. Hu, Y. Peng, High temperature sensitivity phosphor based on an old material: red emitting H_3BO_3 flux assisted $CaTiO_3$:Pr^{3+}, J. Lumin. 214 (2019), 116528 https://doi.org/10.1016/j.jlumin.2019.116528.
[35] K.K. Markose, R. Anjana, A. Antony, M.K. Jayaraj, Synthesis of Yb^{3+}/Er^{3+} co-doped Y_2O_3, YOF and YF_3 UC phosphors and their application in solar cell for sub-bandgap photon harvesting, J. Lumin. 204 (2018) 448–456, https://doi.org/10.1016/j.jlumin.2018.08.005.
[36] NIST (National Institute of Standards and Technology), JARVIS-DFT (n.d.), https://jarvis.nist.gov/jarvisdft/.
[37] G. Li, J. Lin, Phosphors for Field Emission Display: Recent Advances in Synthesis, Improvement, and Luminescence Properties, 2016, https://doi.org/10.1007/978-3-662-52771-9.
[38] X. Liu, C. Lin, J. Lin, White light emission from Eu^{3+} in $CaIn_2O_4$ host lattices, Appl. Phys. Lett. (2007), 081904, https://doi.org/10.1063/1.2539632.
[39] T. Yamase, T. Kobayashi, M. Sugeta, H. Naruke, Europium(III) luminescence and intramolecular energy transfer studies of polyoxometalloeuropates, J. Phys. Chem. A 101 (1997) 5046–5053.
[40] R.G. Geitenbeek, H.W. De Wijn, A. Meijerink, Non-Boltzmann luminescence in $NaYF_4$:Eu^{3+}: implications for luminescence thermometry, Phys.Rev. Appl. 10 (2018) 1, https://doi.org/10.1103/PhysRevApplied.10.064006.
[41] P. Serna-Gallén, H. Beltrán-Mir, E. Cordoncillo, Unraveling the superior role of dicarboxylic acids as surface chelators in Eu^{3+}-doped yttrium fluorides: a systematic modulation of the crystal phases and morphologies for highly tuned optical performance, J. Alloys Compd. 883 (2021), 160847, https://doi.org/10.1016/j.jallcom.2021.160847.
[42] R. Nagaraj, P. Suthanthirakumar, R. Vijayakumar, K. Marimuthu, Spectroscopic properties of Sm^{3+} ions doped Alkaliborate glasses for photonics applications, Spectrochim. Acta Mol. Biomol. Spectrosc. 185 (2017) 139–148, https://doi.org/10.1016/j.saa.2017.05.048.
[43] R. Nagaraj, A. Raja, S. Ranjith, Synthesis and luminescence properties of novel red-emitting Eu^{3+} ions doped silicate phosphors for photonic applications, J. Alloys Compd. 827 (2020), 154289, https://doi.org/10.1016/j.jallcom.2020.154289.
[44] R. Jagannathan, S.P. Manoharan, R.P. Rao, R.L. Narayanan, N. Rajaram, Colour coordinates of some photoluminescent materials, Bull. Electrochem. 4 (1988) 597–600.
[45] B. Rigg, Colour description/specification systems, in: J.H. Xin (Ed.), Total Colour Management in Textiles, Woodhead Publishing Limited, 2006, pp. 22–43, https://doi.org/10.1533/9781845691080.22.
[46] M.R. Luo, Encyclopedia of Science and Technology, Springer, 2016, https://doi.org/10.1108/rr.2002.16.3.27.138.
[47] K.R. J.T, GoCIE V2, 2009. http://faculty.iitr.ac.in/~krjt8fcy/index.html.
[48] P. Patil, CIE Coordinate Calculator, 2022. https://www.mathworks.com/matlabcentral/fileexchange/29620-cie-coordinate-calculator.
[49] OriginLab Tecnhical Support, Chromaticity Diagram, 2022. https://www.originlab.com/fileExchange/details.aspx?fid=446.
[50] P. Babu, C.K. Jayasankar, Optical spectroscopy of Eu^{3+} ions in lithium borate and lithium fluoroborate glasses, Phys. B Condens. Matter 279 (2000) 262–281, https://doi.org/10.1016/S0921-4526(99)00876-5.
[51] K. Vuković, M. Medić, M. Sekulić, M.D. Dramićanin, Analysis of Eu^{3+} emission from Mg_2TiO_4 nanoparticles by Judd-Ofelt theory, Adv. Condens. Matter Phys. 2015 (2015) 1–7, https://doi.org/10.1155/2015/736517.
[52] E. Marín, A. Calderón, Conversion of wavelength and energy scales and the analysis of optical emission spectra, J. Phys. Chem. Lett. 13 (2022) 8376–8379, https://doi.org/10.1021/acs.jpclett.2c02621.
[53] J. Mooney, P. Kambhampati, Get the basics right: Jacobian conversion of wavelength and energy scales for quantitative analysis of emission spectra, J. Phys. Chem. Lett. 4 (2013) 3316–3318, https://doi.org/10.1021/jz401508t.
[54] I.E. Kolesnikov, A.V. Povolotskiy, D.V. Mamonova, E.Y. Kolesnikov, A. V. Kurochkin, E. Lähderanta, M.D. Mikhailov, Asymmetry ratio as a parameter of Eu^{3+} local environment in phosphors, J. Rare Earths 36 (2018) 474–481, https://doi.org/10.1016/j.jre.2017.11.008.
[55] A.M. Srivastava, M.G. Brik, W.W. Beers, W. Cohen, The influence of nd^0 transition metal cations on the Eu^{3+} asymmetry ratio R and crystal field splitting of $^7F_1$ manifold in pyrochlore and zircon compounds, Opt. Mater. 114 (2021), 110931, https://doi.org/10.1016/j.optmat.2021.110931.
[56] G. Phaomei, W.R. Singh, Effect of solvent on luminescence properties of re-dispersible LaF_3:Ln^{3+} (Ln^{3+} = Eu^{3+}, Dy^{3+}, Sm^{3+} and Tb^{3+}) nanoparticles, J. Rare Earths 31 (2013) 347–355, https://doi.org/10.1016/S1002-0721(12)60284-1.
[57] Z. Yuan, C. Shen, Y. Zhu, A. Bai, J. Wang, Y. Liu, Y. Lyu, Multiple morphologies of YF_3:Eu^{3+} microcrystals: microwave hydrothermal synthesis, growth mechanism and luminescence properties, Ceram. Int. 42 (2016) 1513–1520, https://doi.org/10.1016/j.ceramint.2015.09.099.
[58] M.M. Lezhnina, T. Jüstel, H. Kätker, D.U. Wiechert, U.H. Kynast, Efficient luminescence from rare-earth fluoride nanoparticles with optically functional shells, Adv. Funct. Mater. 16 (2006) 935–942, https://doi.org/10.1002/adfm.200500197.
[59] B.R. Judd, Optical absorption intensities of rare-earth ions, Phys. Rev. 127 (1962) 750–761, https://doi.org/10.1103/PhysRev.127.750.
[60] G.S. Ofelt, Intensities of crystal spectra of rare-earth ions, J. Chem. Phys. 37 (1962) 511–520, https://doi.org/10.1063/1.1701366.
[61] M.P. Hehlen, M.G. Brik, K.W. Krämer, 50th anniversary of the Judd-Ofelt theory: an experimentalist's view of the formalism and its application, J. Lumin. 136 (2013) 221–239, https://doi.org/10.1016/j.jlumin.2012.10.035.
[62] G. Yao, C. Lin, Q. Meng, P. Stanley May, M.T. Berry, Calculation of Judd-Ofelt parameters for Er^{3+} in β-$NaYF_4$:Yb^{3+}, Er^{3+} from emission intensity ratios and diffuse reflectance spectra, J. Lumin. 160 (2015) 276–281, https://doi.org/10.1016/j.jlumin.2014.12.025.
[63] M.J. Weber, Probabilities for radiative and nonradiative decay of Er^{3+} in LaF_3, Phys. Rev. 157 (1967) 262–272, https://doi.org/10.1103/PhysRev.157.262.
[64] W.T. Carnall, P.R. Fields, K. Rajnak, Electronic energy levels in the trivalent lanthanide aquo ions. I. Pr^{3+}, Nd^{3+}, Pm^{3+}, Sm^{3+}, Dy^{3+}, Ho^{3+}, Er^{3+}, and Tm^{3+}, J. Chem. Phys. 49 (1968) 4424–4442.
[65] C.K. Jørgensen, R. Reisfeld, Judd-Ofelt parameters and chemical bonding, J. Less Common. Met. 93 (1983) 107–112, https://doi.org/10.1016/0022-5088(83)90454-X.
[66] B.M. Walsh, Judd-Ofelt theory: principles and practices, in: B. Di Bartolo, O. Forte (Eds.), Advances in Spectroscopy for Lasers and Sensing, Springer, Dordrecht, 2006, pp. 403–433, https://doi.org/10.1007/1-4020-4789-4_21.
[67] L. Smentek, Judd-ofelt theory–the golden (and the only one) theoretical tool of f-electron spectroscopy, in: M. Dolg (Ed.), Computational Methods in Lanthanide and Actinide Chemistry, Wiley, 2015, pp. 241–268.
[68] A. Ćirić, S. Stojadinović, M.G. Brik, M.D. Dramićanin, Judd-Ofelt parametrization from emission spectra: the case study of the Eu^{3+} $^5D_1$ emitting level, Chem. Phys. 528 (2020), 110513, https://doi.org/10.1016/j.chemphys.2019.110513.
[69] D.K. Patel, B. Vishwanadh, V. Sudarsan, S.K. Kulshreshtha, Difference in the nature of Eu^{3+} environment in Eu^{3+}-doped $BaTiO_3$ and $BaSnO_3$, J. Am. Ceram. Soc. 96 (2013) 3857–3861, https://doi.org/10.1111/jace.12596.
[70] C. de Mello Donegá, S.A. Junior, G.F. de Sá, Synthesis, luminescence and quantum yields of Eu(III) mixed complexes with 4,4,4-trifluoro-1-phenyl-1,3-butanedione and 1,10-phenanthroline-*N*-oxide, J. Alloys Compd. 250 (1997) 422–426, https://doi.org/10.1016/S0925-8388(96)02562-5.
[71] P. Serna-Gallén, H. Beltrán-Mir, E. Cordoncillo, A.R. West, R. Balda, J. Fernández, Site-selective symmetries of Eu^{3+}-doped $BaTiO_3$ ceramics: a structural elucidation by optical spectroscopy, J. Mater. Chem. C 7 (2019) 13976–13985, https://doi.org/10.1039/c9tc03987b.
[72] M. İlhan, M.K. Ekmekçi, İ.Ç. Keskin, Judd-Ofelt parameters and X-ray irradiation results of MNb_2O_6:Eu^{3+} (M = Sr, Cd, Ni) phosphors synthesized via a molten salt method, RSC Adv. 11 (2021) 10451–10462, https://doi.org/10.1039/d0ra10834k.
[73] J.D.L. Dutra, T.D. Bispo, R.O. Freire, LUMPAC lanthanide luminescence software: efficient and user friendly, J. Comput. Chem. 35 (2014) 772–775, https://doi.org/10.1002/jcc.23542.
[74] A. Ćirić, S. Stojadinović, M. Sekulić, M.D. Dramićanin, JOES: an application software for Judd-Ofelt analysis from Eu^{3+} emission spectra, J. Lumin. 205 (2019) 351–356, https://doi.org/10.1016/j.jlumin.2018.09.048.
[75] J.J. Stewart, MOPAC2012. http://openmopac.net/, 2012.
[76] F. Neese, The ORCA program system, WIREs Comput. Molecul. Sci. 2 (2012) 73–78, https://doi.org/10.1002/wcms.81.
[77] A. Ćirić, Ł. Marciniak, M.D. Dramićanin, Self-referenced method for the Judd–Ofelt parametrisation of the Eu^{3+} excitation spectrum, Sci. Rep. 12 (2022) 1–10, https://doi.org/10.1038/s41598-021-04651-4.
[78] M.J. Bin Murshed Leon, S. Abedin, M.A. Kabir, A photonic crystal fiber for liquid sensing application with high sensitivity, birefringence and low confinement loss, Sensor. Int. 2 (2021), 100061, https://doi.org/10.1016/j.sintl.2020.100061.
[79] L. Cao, G. Peng, W. Liao, T. Yan, X. Long, N. Ye, A microcrystal method for the measurement of birefringence, CrystEngComm 22 (2020) 1956–1961, https://doi.org/10.1039/c9ce01934k.
[80] M. Zhao, Y. Sun, Y. Wu, D. Mei, S. Wen, T. Doert, NaTePO5, $SrTeP_2O_8$ and $Ba_2TeP_2O_9$: three tellurite-phosphates with large birefringence, J. Alloys Compd. 854 (2021), https://doi.org/10.1016/j.jallcom.2020.157243, 0–10.
[81] R.D. Shannon, R.X. Fischer, Empirical electronic polarizabilities of ions for the prediction and interpretation of refractive indices: oxides and oxysalts, Am. Mineral. 101 (2016) 2288–2300, https://doi.org/10.2138/am-2016-5730.
[82] R.D. Shannon, R.X. Fischer, Empirical electronic polarizabilities in oxides, hydroxides, oxyfluorides, and oxychlorides, Phys. Rev. B Condens. Matter 73 (2006) 1–28, https://doi.org/10.1103/PhysRevB.73.235111.
[83] R.C. Shannon, B. Lafuente, R.D. Shannon, R.T. Downs, R.X. Fischer, Refractive indices of minerals and synthetic compounds, Am. Mineral. 102 (2017) 1906–1914, https://doi.org/10.2138/am-2017-6144.
[84] M.N. Polyanskiy, Refractive index database, (n.d.), https://refractiveindex.info.

[85] P. Villars, K. Cenzual (Eds.), C-Y_2O_3 (Y_2O_3 Rt) Crystal Structure: Datasheet from "PAULING FILE Multinaries Edition – 2012''', Springer Materials, 2012. https://materials.springer.com/isp/crystallographic/docs/sd_0305868 (n.d.).
[86] P. Villars, K. Cenzual (Eds.), $Y_3Al_5O_{12}$ Crystal Structure: Datasheet from "PAULING FILE Multinaries Edition – 2012''', Springer Materials, 2012. https://materials.springer.com/isp/crystallographic/docs/sd_0309606 (n.d.).
[87] P. Villars, K. Cenzual (Eds.), $MgAl_2O_4$ Crystal Structure: Datasheet from "PAULING FILE Multinaries Edition – 2012''', Springer Materials, 2012. https://materials.springer.com/isp/crystallographic/docs/sd_0310018 (n.d.).
[88] P. Villars, K. Cenzual (Eds.), LaF_3 Crystal Structure: Datasheet from "PAULING FILE Multinaries Edition – 2012''', Springer Materials, 2012. https://materials.springer.com/isp/crystallographic/docs/sd_0379018 (n.d.).
[89] J.G. Li, X. Wang, K. Watanabe, T. Ishigaki, Phase structure and luminescence properties of Eu^{3+}-doped TiO_2 nanocrystals synthesized by Ar/O_2 radio frequency thermal plasma oxidation of liquid precursor mists, J. Phys. Chem. B 110 (2006) 1121–1127, https://doi.org/10.1021/jp053329l.
[90] Ž. Antić, R.M. Krsmanović, M.G. Nikolić, M. Marinović-Cincović, M. Mitrić, S. Polizzi, M.D. Dramićanin, Multisite luminescence of rare earth doped TiO_2 anatase nanoparticles, Mater. Chem. Phys. 135 (2012) 1064–1069, https://doi.org/10.1016/j.matchemphys.2012.06.016.
[91] D. Avram, A.A. Patrascu, M.C. Istrate, B. Cojocaru, C. Tiseanu, Lanthanide doped TiO_2: coexistence of discrete and continuous dopant distribution in anatase phase, J. Alloys Compd. 851 (2021), 156849, https://doi.org/10.1016/j.jallcom.2020.156849.
[92] R.D. Shannon, Revised effective ionic radii and systematic studies of interatomic distances in halides and chalcogenides, Acta Crystallogr. A. 32 (1976) 751–767, https://doi.org/10.1107/S0567739476001551.
[93] Y.Q. Jia, Crystal radii and effective ionic radii of the rare earth ions, J. Solid State Chem. 95 (1991) 184–187, https://doi.org/10.1016/0022-4596(91)90388-X.
[94] C. Cascales, R. Balda, S. García-Revilla, L. Lezama, M. Barredo-Zuriarrain, J. Fernández, Site symmetry and host sensitization-dependence of Eu^{3+} real time luminescence in tin dioxide nanoparticles, Opt Express 26 (2018), 16155, https://doi.org/10.1364/oe.26.016155.
[95] H. Lösch, A. Hirsch, J. Holthausen, L. Peters, B. Xiao, S. Neumeier, M. Schmidt, N. Huittinen, A spectroscopic investigation of Eu^{3+} incorporation in $LnPO_4$ (Ln = Tb, $Gd_{1-x}Lu_x$, $x = 0.3, 0.5, 0.7, 1$) ceramics, Front. Chem. 7 (2019) 1–16, https://doi.org/10.3389/fchem.2019.00094.
[96] V.P. Tuyen, T. Hayakawa, M. Nogami, J.R. Duclre, P. Thomas, Fluorescence line narrowing spectroscopy of Eu^{3+} in zinc-thallium-tellurite glass, J. Solid State Chem. 183 (2010) 2714–2719, https://doi.org/10.1016/j.jssc.2010.08.025.
[97] R. Balda, J. Fernández, J. Adam, Time-resolved fluorescence-line narrowing and energy-transfer studies in a-doped fluorophosphate glass, Phys. Rev. B Condens. Matter 54 (1996) 12076–12086, https://doi.org/10.1103/PhysRevB.54.12076.